NASA TECHNICAL NOTE

NASA TN D-5238

c. 1

NASA TN D-5238

METHODS FOR PREDICTING SPACECRAFT-WINDOW-INDUCED LINE-OF-SIGHT DEVIATIONS

by Kenneth C. White and Burnett L. Gadeberg

Ames Research Center
Moffett Field, Calif.

NATIONAL AERONAUTICS AND SPACE ADMINISTRATION • WASHINGTON, D. C. • JULY 1969

METHODS FOR PREDICTING SPACECRAFT-WINDOW-INDUCED LINE-OF-SIGHT DEVIATIONS

By Kenneth C. White and Burnett L. Gadeberg

Ames Research Center
Moffett Field, Calif.

NATIONAL AERONAUTICS AND SPACE ADMINISTRATION

For sale by the Clearinghouse for Federal Scientific and Technical Information
Springfield, Virginia 22151 – CFSTI price $3.00

METHODS FOR PREDICTING SPACECRAFT-WINDOW-INDUCED LINE-OF-SIGHT DEVIATIONS

By Kenneth C. White and Burnett L. Gadeberg

Ames Research Center

SUMMARY

Methods have been developed for predicting angular line-of-sight deviations induced by spacecraft windows. Line-of-sight deviations are defined herein as angular deviations of the lines of sight as they pass through the spacecraft window. The methods require an accurate description of the shape of the window surface and a set of ray-trace equations.

The description of the window surface shape requires an accurate knowledge of the flatness distribution over the whole window surface, the parallelism between the surfaces of the window, and the surface deformation due to pressure loading. The window surface flatness distribution and the parallelism between surfaces are determined from interference photographs of the window. Pressure deformations of windows with known edge support conditions are computed by means of known analytical solutions or a finite element structural analysis computer program. Pressure deformations of windows with unknown edge conditions are determined experimentally from interference photographs of the window surfaces.

The prediction methods were used to compute the line-of-sight (LOS) deviations for a Gemini spacecraft window. The edge conditions were: (1) the actual Gemini edges, (2) idealized clamped edges, and (3) idealized simply supported edges. LOS deviations computed for the three edge conditions included the combined effects of window surface nonflatness, wedge angle, and pressure deformation, as well as index-of-refraction difference of the light transmission media inside and outside the spacecraft. The deviations are functions of both LOS orientation and incidence position on the window. Deviations up to 20 arcsec were encountered.

The computed LOS deviations were compared with experimentally measured LOS deviations to assess the validity of the methods developed. A detailed statistical analysis of the differences between computed and experimentally measured data indicated that the results agreed to within 2 arcsec mean difference and 4 arcsec standard deviation. The methods developed will provide accurate prediction of spacecraft window-induced LOS deviations if the window surface shapes are known with sufficient accuracy.

INTRODUCTION

On-board navigation systems that derive their basic inputs from optical measurements made through a spacecraft window have been considered for manned space flight. For example, on-board navigation concepts that use the hand-held space sextant have been studied for backup navigation during the

midcourse, earth-orbital, and orbit-rendezvous phases of the manned translunar mission as well as the interplanetary mission (e.g., refs. 1-4). For navigation, the measurement of interest in the midcourse or earth-orbital phase is the angle between two celestial bodies such as a star and a planet; whereas, during orbit rendezvous, it is the angle between a star and a target spacecraft. These angular navigation measurements are subject to window-induced errors that result from the deviation or bending of the line of sight (LOS) from the sighting targets as they pass through the window. The effect of these navigational errors on a return from Mars mission (by a Venus swingby) is indicated in reference 5, wherein it was concluded that window-induce errors must be determined to within a few seconds of arc. The window as used herein will consist of one or more panes of glass mounted in a frame in the spacecraft structure. Sources of window-induced LOS deviations are: nonflat window surfaces, nonparallel window surfaces, window deformations due to pressure loading, and the differences between the index of refraction of the air inside the spacecraft and the outside space environment.

Walsh, Warner, and Davis (ref. 6) and Warner and Walsh (ref. 7) have made limited exerimental investigations of the LOS deviations for optical and nonoptical quality Gemini spacecraft windows. Koch et al. (ref. 8) made a limited analytic study of the deviations for an elliptical approximation of the Gemini window shape. However, up to this time, no definitive analytic study of spacecraft window-induced LOS deviations has been made.

Gadeberg and White (ref. 9) developed an analysis method for determining window-induced LOS deviations. The method which was utilized in this study consists basically of a ray-trace scheme that will permit tracing of light rays through any type of window system in which the window surface shapes can be described mathematically. The development of the mathematical models for the surface shapes requires accurate knowledge of the window surface deformations due to pressure loading that are critically dependent on window planform shape and window edge mounting conditions. If the window is regular and symmetrical in shape and the edge conditions are known, exact closed form solutions exist for the pressure deformations. If the window is not regular in shape but the edge conditions are known, the pressure deformations can be obtained with a numerical solution. However, if the edge conditions are not known or cannot be readily defined, the pressure deformations must be obtained by some experimental method that would require modification of the analysis method developed in reference 9.

The objectives of this report are to: (1) apply the analysis method of reference 9 to the analysis of LOS deviations associated with a spacecraft window with known edge conditions, nonflatness, and wedge angle; (2) evaluate the accuracy of the analysis method by comparison of results with experimentally measured data; (3) modify the method to permit determination of LOS deviations for a window with unknown edge conditions by obtaining the window surface pressure deformations from interference photographs obtained in the laboratory; (4) evaluate the accuracy of this modified method by applying it to a window with known edge conditions and then comparing the results with those obtained with the basic method; and (5) apply this modified method to the determination of LOS deviations for a spacecraft window with unknown edge conditions and compare the results with experimentally measured data.

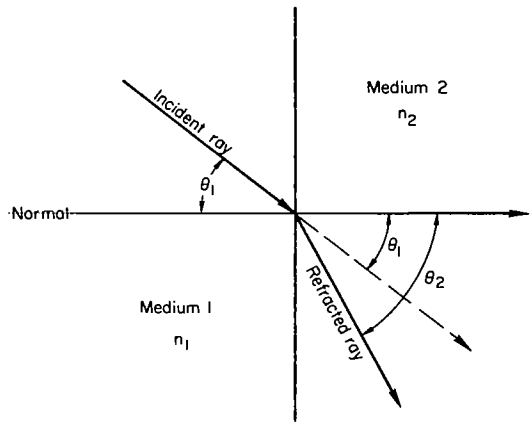

Sketch (a)

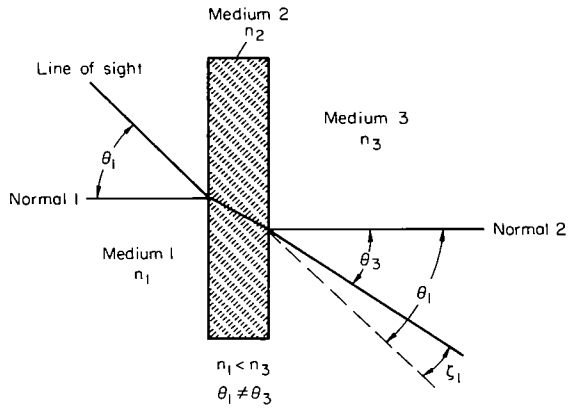

Sketch (b)

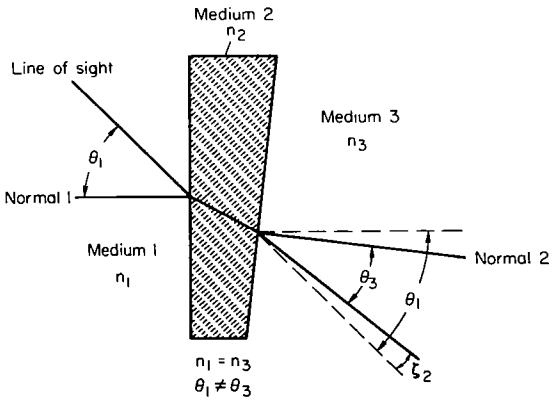

Sketch (c)

The spacecraft window used for all phases of the study is the Gemini spacecraft optical quality window. The window is assumed to have known clamped and simply supported edge conditions for the application of the basic analysis method, and the actual Gemini edges that are difficult to define are used for application of the modified method.

DEVELOPMENT OF METHOD

The presence of the spacecraft window in the path of light rays causes these rays to bend or to be deviated from their original path. Light ray deviations can best be explained by Snell's Law of Refraction, which is illustrated in sketch (a). Snell's law is $n_1 \sin \theta_1 = n_2 \sin \theta_2$, where n_1 is the index of refraction of medium 1, θ_1 is the angle the incident ray makes with the normal to the interface between mediums 1 and 2, n_2 is the index of refraction of medium 2, and θ_2 is the angle the refracted ray in medium 2 makes with the normal. Examination of Snell's law indicates that a ray of light will be deviated through some angle as it passes through a spacecraft window if the media on either side of the window have different indices of refraction; or if the media are the same, a light ray will be deviated if it intersects the window surfaces at points where the normals to the surfaces are not parallel. Ray deviations would also result from changes in the index of refraction within the glass itself. However, in this study it was assumed that the index of refraction remains constant throughout the glass. Two examples of light ray deviations are illustrated in sketches (b) and (c) where the cross-hatched areas represent windowpanes.

Sketch (b) illustrates light ray deviation due to differences in the media on either side of the windowpane. In this case, the window surfaces are

perfectly flat and parallel, but medium 3 is more dense than medium 1, and, therefore, the index of refraction n_3 is greater than n_1. It is evident from Snell's law that the angles θ_1 and θ_3 are not equal and that the light ray is deviated by the angle ξ_1. This type of deviation occurs in an orbiting spacecraft where the index of refraction is larger for the air inside the spacecraft cabin than for the space vacuum outside.

Sketch (c) illustrates light ray deviation when the ray intersects the window surfaces at points where the normals to the surfaces are different. In the example shown, media 1 and 3 are identical, and the window surfaces are flat but not parallel. The angles θ_1 and θ_2 are not equal because the window surfaces are not parallel, and the light rays intersect the window surfaces at points where the normals 1 and 2 are not parallel and the LOS is deviated by the angle ξ_2. Light ray deviations will also result if the ray intersects the window surfaces at points where the window surfaces are parallel but not flat, as when the window is subjected to pressure loading, or if the surfaces are both nonflat and nonparallel. For the actual spacecraft window, the surface shape must be known accurately at all points. An accurate determination of the surface shape requires knowledge of the window edge conditions, pressure loading on the window, specifications of manufacture, and nominal window planform. The problem becomes more complex because the planform of the window is quite often neither geometrically regular nor symmetrical; thus, the surface shapes of the window when subjected to pressure loading are not symmetrical.

The preceding presents a simplified discussion of the causes of the light ray deviations. In this study, LOS originating from some reference point inside a spacecraft are traced toward the outside of the spacecraft. Thus, the LOS travel in the opposite direction from light rays that emanate from some celestial body and travel toward the spacecraft. The theory used to determine the LOS deviations for an actual spacecraft window is the same as that for finding light ray deviations, except that the tracing is done in a reverse direction. The ray trace equations and digital computer program used in this study were developed by Gadeberg and White (ref. 9). The method is illustrated by the flow diagram in figure 1. A particular spacecraft is assumed with a given pressure and temperature environment. The given pressure loads and temperature variations over the spacecraft structure will cause structural deformations, which, in turn, will impose forces and moments on the window frame, and the window will be deformed. In this study, deformations due to window temperature were not considered since preliminary calculations (ref. 8) indicated they were negligible in comparison to the pressure deformations. Window deformation due to pressure loading was determined in two ways. When the window edge conditions were known (i.e., idealized edge supports), a structural analysis, digital computer program was used. The inputs to the program are indicated in the diagram. When the window edge conditions were not known, the surface deformations were measured in the laboratory from interference photographs of the window.

It was also necessary to determine the window surface nonflatness and the wedge angle (i.e., the angle between nonparallel window surfaces) that result from the manufacturing process. These characteristics were also obtained from interference photographs.

The window surface nonflatness and the wedge angle were combined with the window deformations caused by pressure loading to give numerical values of the total deformation at discrete points on the window surface. The deformations were then put into a computer program, which, in turn, computed a model of the window surface shape.

The computed models of the window surface shapes and the window design properties were used in the ray trace program to calculate the LOS deviations. The LOS deflected by the window was then compared with the undeviated LOS to obtain the sighting error induced by the window.

To summarize, the method for determining the LOS deviations is as follows, given the spacecraft and window configuration: (1) window surface pressure deformations are determined either analytically or experimentally; (2) window surface anomalies of manufacture are obtained experimentally; (3) pressure deformations and anomalies of manufacture are used to obtain a mathematical model of the window surface shapes; and (4) rays corresponding to LOS are traced through the window to determine angular LOS deviations.

COMPUTATIONAL PROCEDURES

Window Surface Modeling

A ray may be traced through a spacecraft window system only if the normals to the window surfaces at the points of intersection are accurately known. To find the normals, the surfaces must be described in some meaningful mathematical form. Therefore, a key step in the application of the analytic method is the mathematical modeling of the window surface shape. A convenient method of modeling the surface shape is to describe it in terms of its variations from the xy-plane of a cartesian coordinate system. Then, the variation from the plane in the z-direction, denoted by ΔZ, at any point (x, y) on the plane can be expressed as a function of x and y. This functional relationship is obtained by means of the function approximation technique described in reference 9. In this technique, the deflections, ΔZ, at discrete points are fitted with a smooth three-dimensional curve that provides a polynomial approximation to the surface. The deflections ΔZ are expressed as nth-degree mixed polynomials in x and y as follows:

$$Z = m_{11}x^n y^n + m_{12}x^{n-1}y^n + \ldots + m_{n,n+1}y + m_{n+1,n+1}$$

Or, in matrix form:

$$\Delta Z = \bar{Y}^T M \bar{X} \qquad (1)$$

where

$$\bar{Y}^T = \begin{bmatrix} y^n & y^{n-1} y^{n-2} & \cdots & y & 1 \end{bmatrix}, \qquad \bar{X} = \begin{bmatrix} x^n \\ x^{n-1} \\ x^{n-2} \\ \cdot \\ \cdot \\ \cdot \\ x \\ 1 \end{bmatrix}$$

and M, called the mathematical model of the window surface, is the matrix of the coefficients of the nth-degree mixed polynomial in x and y.

In this study, a fourth-degree mixed polynomial gave an excellent approximation to the window surface shapes. Once the window surfaces were described mathematically in this manner, the unit vector normal to the surface at a given point (x, y) was obtained by evaluating the gradient of the surface at that point. Equation (1) is written in the form $\Delta Z - \bar{Y}^T M \bar{X} = 0$, then F (x, y, z) is set equal to the left-hand side of the equation, and the unit vector normal to the surface F is given by:

$$\hat{N} = \frac{\bar{\nabla} F}{|\bar{\nabla} F|} = \frac{\left(\frac{\partial F}{\partial x}\right)\hat{i} + \left(\frac{\partial F}{\partial y}\right)\hat{j} + \left(\frac{\partial F}{\partial z}\right)\hat{k}}{\sqrt{\left|\frac{\partial F}{\partial x}\right|^2 + \left|\frac{\partial F}{\partial y}\right|^2 + \left|\frac{\partial F}{\partial z}\right|^2}} \tag{2}$$

where

$$\frac{\partial F}{\partial x} = -\bar{Y}^T M \frac{d\bar{X}}{dx}\ ; \qquad \frac{\partial F}{\partial y} = -\frac{d\bar{Y}^T}{dy} M \bar{X}\ ; \qquad \frac{\partial F}{\partial z} = 1$$

and

$$\frac{d\bar{X}}{dx} = \begin{bmatrix} nx^{n-1} \\ (n-1)x^{n-2} \\ \cdot \\ \cdot \\ \cdot \\ 2x \\ 1 \\ 0 \end{bmatrix}\ ; \qquad \frac{d\bar{Y}^T}{dy} = \begin{bmatrix} ny^{n-1} & (n-1)y^{n-2} & \cdots & 2y & 1 & 0 \end{bmatrix}$$

Pressure deformations.- As noted previously, the math modeling program requires an accurate knowledge of the window surface deformations due to pressure loading.

If the window is symmetrical and regular in shape, the deformations can be calculated by means of flat-plate theory, and equations are given in the literature for idealized clamped and simply supported edge conditions.

If the window is not regular or symmetrical in shape but the edge conditions are known (that is, the deflections and angular rotations of the window edges are known), the pressure deformations can be computed by means of a digital computer structural analysis program, SAMIS (ref. 10). To check the accuracy of the SAMIS program the pressure deformations computed from the closed-form equation for a single pane window with an elliptic planform and clamped edge conditions were compared with deformations computed by the SAMIS program (a numerical approximation to the exact closed-form solutions). These deformations are presented in figure 2 as a function of position along the semiminor axis of the ellipse. The deformations differ less than 8×10^{-5} inch between the exact and SAMIS computer solutions, while the slopes of the window surface differ less than one arcsec. Similar agreement was obtained for the elliptic window with simply supported edge conditions. This good agreement indicates that if the window edge conditions are known, the SAMIS program correctly predicts the deformations for regular window shapes. It is presumed that the SAMIS program will also accurately predict the deformations for those shapes that differ a moderate amount from the regular shapes.

If the window edge conditions are not known or cannot be readily defined mathematically, numerical solutions for the deformations cannot be formulated. Therefore, a different technique is required for determining the window surface pressure deformations. One technique is to obtain interference photographs of the window surfaces in the laboratory and then compute the deformations from the interference fringes on the photographs. The fringe pattern is similar to a geographic contour map. The ring near the center of the fringe pattern corresponds to the maximum deformation, and the outer rings represent contours of constant deformation or elevation.

The pressure deformations are determined from the number of fringes relative to the fringe near the center. Counting fringes near the edges is tedious because the fringes are very close together and difficult to discern; thus, good magnification and photo contrast are very important. Despite these difficulties, such photographs have been used successfully.

Surface flatness and wedge angle.- To define the surface shape completely, the mathematical modeling program also requires a knowledge of the nonflatness of the window surfaces and the window-wedge angle. Surface imperfections, which result from the manufacturing process, are measured in the laboratory from interference photographs of the window. The magnitude of the deviation from flat is a function of the number of fringe lines that cross a particular straight line drawn on the interference pattern. The angle between the nonparallel surfaces of a windowpane is obtained from the spacing

of the fringes rather than from their straightness. The laboratory apparatus and techniques for obtaining information from the photographs are explained in detail in reference 7.

Ray Tracing

Ray trace coordinate system.- The coordinate system used in the ray trace analysis is illustrated in sketch (d). The innermost surface of the spacecraft window is assumed to lie in the xy-plane. The positive z-axis is toward the outside of the spacecraft. The incident and refracted rays and their orientation angles are also illustrated in the sketch. The vector $\hat{I}$ is the unit vector in the direction of the incident ray. The azimuth angle, α_i, is defined as the angle in the xy-plane between the positive x-axis and the projection, $\hat{I}_p$, of $\hat{I}$ onto the xy-plane. The elevation angle, δ_i, is the angle between $\hat{I}$ and $\hat{I}_p$. The incidence angle, θ, not shown, is the complement of δ_i. The unit vector, $\hat{R}$, is in the direction of the refracted ray, which emerges from the outermost window surface. The azimuth angle, α_r, is the angle in the xy-plane between the positive x-axis and the projection $\hat{R}_p$, of $\hat{R}$ onto the xy-plane. The azimuth angles α_i and α_r are measured from the positive x-axis toward the positive y-axis and vary from 0° to 360°. The elevation angles δ_i and δ_r are measured from the projected vectors $\hat{I}_p$ and $\hat{R}_p$ toward the positive z-axis and vary from 0° to 90°.

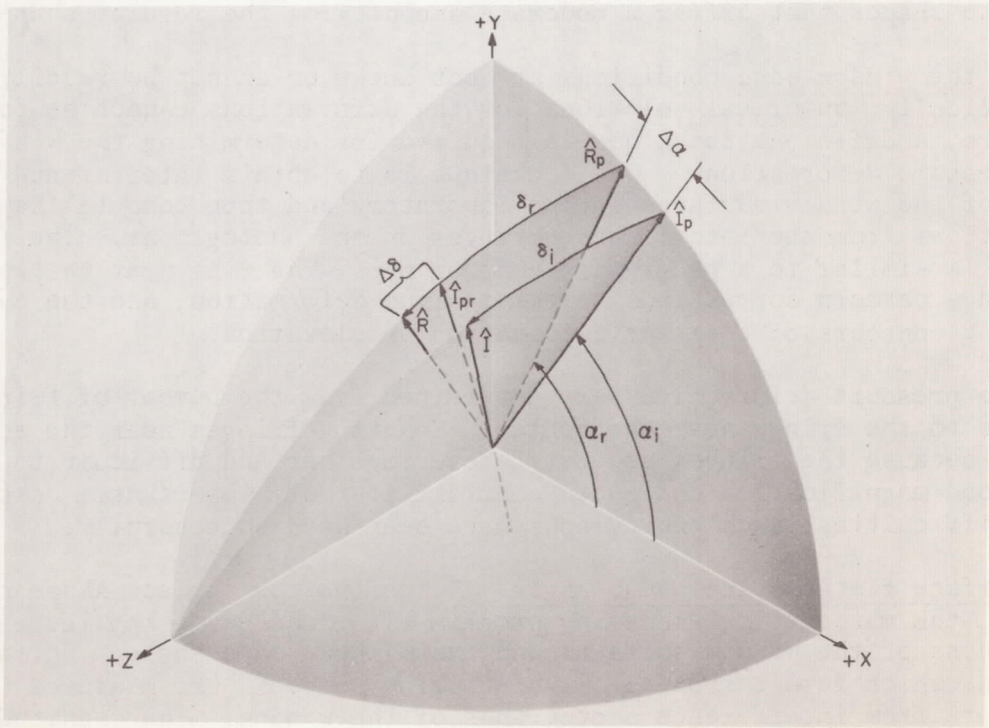

Sketch (d)

Two LOS deviations, $\Delta\alpha$ and $\Delta\delta$, are also defined in sketch (d). The change in elevation angle called the in-plane deviation is defined as $\Delta\delta = (\delta_i - \delta_r)$ and lies in the plane formed by $\hat{R}$, $\hat{R}_p$, and the z-axis. The

change in azimuth angle called the out-of-plane deviation is defined as $\Delta\alpha = (\alpha_i - \alpha_r)$ and is the angle out of the plane formed by $\hat{R}$ and $\hat{R}_p$.

Ray trace equation.- For mathematical convenience and ease in computation, Snell's law, the basic equation for ray tracing, is expressed in vector form:

$$\hat{R} = \left(\frac{n_1}{n_2}\right)\hat{I} + \left\{\sqrt{1 - \left(\frac{n_1}{n_2}\right)^2 [1 - (\hat{I} \cdot \hat{N})^2]} - \left(\frac{n_1}{n_2}\right)(\hat{I} \cdot \hat{N})\right\}\hat{N} \tag{3}$$

where $\hat{R}$ and $\hat{I}$ are unit vectors in the direction of the refracted and incident ray, respectively. The unit vector, $\hat{N}$, given by equation (2) is the normal to the window surface at the point of intersection of the incident ray with the interface between media 1 and 2, and n_1 and n_2 are the refractive indices of the media containing $\hat{I}$ and $\hat{R}$, respectively. The vector $\hat{I}$ is given by the following equation:

$$\hat{I} = \cos \delta_i \cos \alpha_i \hat{i} + \cos \delta_i \sin \alpha_i \hat{j} + \sin \delta_i \hat{k} \tag{4}$$

where $\hat{i}$, $\hat{j}$, and $\hat{k}$ are unit vectors in the direction of the x, y, and z axes, respectively.

The point of intersection of a ray with a window surface is determined by the iteration scheme described in reference 9. This scheme is necessary because the intersection of a ray with this surface cannot be obtained with a closed-form mathematical solution. The scheme converges rapidly and generally requires less than 10 iteration steps.

Equations (1), (2), and (3) and the iteration scheme for determining the points of intersection are the mathematical tools used to compute the LOS deviation.

Digital computer program.- The ray trace equations (1), (2), and (3) and the iteration scheme were programmed on a digital computer. This program was designed to trace rays through a multipane spacecraft window of any size or shape. The incident ray emanates from a reference point which may be the eyeball of an observer or some point on an optical sighting instrument. The reference point will be inside the spacecraft or on the innermost glass surface. The x, y, z coordinates of the reference point and the incident ray azimuth and elevation angles are put into the program, which then traces the ray through the window. The LOS deviation is the angular difference between the incident and refracted rays. Other required program inputs are the number of windowpanes, the index of refraction of each medium that the ray traverses, the math models that describe each surface of each pane, and the location of the reference planes. These planes correspond to the interfaces between air and glass if all the window surfaces are perfectly flat and parallel to the xy-plane of the window coordinate system. The ray trace equations permit study of spacecraft windows that have asymmetrically deformed surfaces.

The computer program is written in Fortran IV and was used on an IBM 7094 computer system.

Description of a ray trace.- A two-dimensional ray trace through a typical spacecraft window made up of three panes of glass (two panes are deflected) is shown in sketch (e). As noted previously, the ray, $\bar{I}$, begins at point A. The intersection of $\bar{I}$ with the first reference plane, RP1, at point B is computed by the method given in reference 9. With point B known, the iteration scheme described in reference 9 can be used to compute point C at which $\bar{I}$ intersects the first window surface. The normal to the surface at point C is computed from the gradient of the surface at that point. Then, Snell's law (eq. (3)) is used to trace the refracted ray through the first pane. The intersection of the refracted ray with the plane RP2 at point D is then computed. Another iteration is performed to find the intersection, point E. The normal to the second surface at point E is then computed and the refracted ray becomes the incident ray for pane 2, and the computation procedure is repeated until the refracted ray, $\bar{R}$, has passed through the final surface at point K. The azimuth and elevation angles of $\bar{R}$ are then computed and compared with those for $\bar{I}$ to give the angular LOS deviations $\Delta\alpha$ and $\Delta\delta$. This is a summary of the ray trace as it is mechanized in the computer program. The procedure for tracing rays through other than three panes is essentially the same as in the preceding discussion with only a change in the number of computation steps, depending upon the number of panes involved.

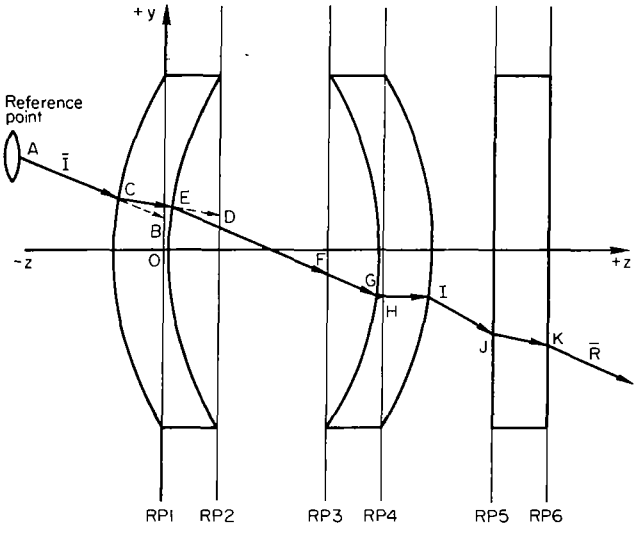

Sketch (e)

APPLICATION OF ANALYSIS METHODS TO A SPACECRAFT WINDOW

The experimental and analysis methods that have been discussed have been applied to the Gemini window. The window was chosen because it was a typical example of spacecraft window technology and because an actual window and frame were available for experimental work, thus providing the opportunity to obtain experimental data to verify the analysis work.

Determination of Window Surface Math Models

Window geometry and properties.- The size and shape of the Gemini right-hand window is illustrated in sketch (f). Sketch (g) shows the window

as it is oriented with respect to the previously described coordinate system. The coordinate system originates at the center of the 6-inch-diameter optical area through which any optical sightings would be made.

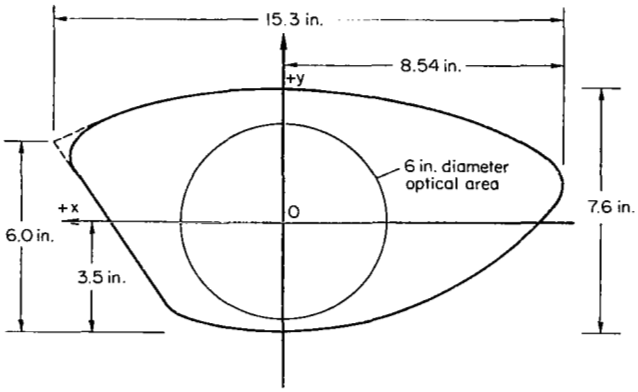

Sketch (f)

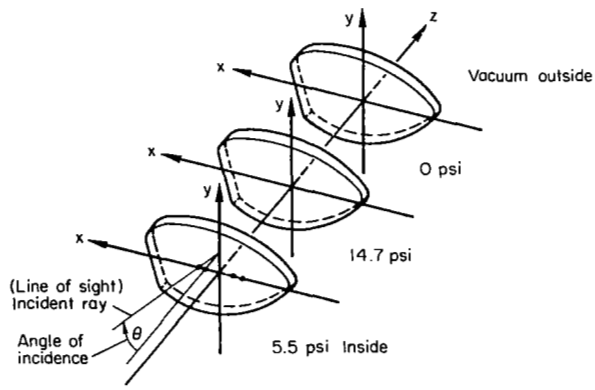

Sketch (g)

The window consists of three panes of fused silica glass (sketch (g)). The inner two panes are 0.38 inch thick, and the outer pane is 0.33 inch thick. The inner two panes are 0.156 inch apart and the outer pane is 1.234 inches from the middle pane. The pressure environment is also indicated in the sketch. Air pressure in the spacecraft cabin is 5.5 psi. The pressure between the inner and middle panes is 14.7 psi. Vacuum exists between the middle and outer panes and outside the spacecraft.

For computation of the window deformation and LOS deviations, it was assumed that the fused silica glass has the following physical properties:

Young's modulus	$E = 9.6\times10^{6}$ lb/in.^{2}
Poisson's ratio	$\nu = 0.19$
Refractive index	$n_D = 1.459$

The specifications governing the optical finish of the window requires each surface of each pane to be flat to within 5 wavelengths (λ) of sodium D light in the 6-inch-diameter optical area and to be uniform within 1/8 wavelength. Surfaces of each pane were specified to be parallel to within 4 arcsec (i.e., wedge angle = 4 arcsec). The windowpanes used in the experimental study had a maximum nonflatness of approximately 2λ, with the surfaces generally convex toward the inside of the spacecraft. Because LOS deviations due to this small nonflatness were generally less than 1 arcsec, nonflatness was not included in the math models of the window surfaces. The average wedge angle for each windowpane used in the study was slightly over 2 arcsec, with the thick part of the wedge toward the top of the window. These wedge angle characteristics of the actual window were included in the calculations.

Pressure deformation calculations.- Pressure deformations of the Gemini window surfaces were obtained for three separate edge conditions. Deformations for clamped and simply supported edge conditions were computed by the

structural analysis program (SAMIS) discussed previously. However, the actual Gemini window edge conditions are very difficult to define, and therefore the pressure deformations were measured from interference photographs obtained in the laboratory. The pressure deformations were then used as one input to the modeling program. Models were obtained for the three edge conditions previously mentioned, and were then used with the ray trace program to compute the LOS deviations. The LOS deviations will be discussed in detail in the next section.

Procedure for Validation of Analysis Methods

LOS deviations induced by the Gemini window have been calculated by the two previously discussed methods of analysis.

The first method permits the analytical determination of LOS deviations for windows with known edge conditions; the window surface deformations due to pressure loading are computed from known exact solutions or from the SAMIS computer program. The second method permits the determination of LOS deviations for windows with unknown edge conditions; the window surface pressure deformations are measured from interference photographs of the window. These methods must be validated to assure accuracy to the order of a few seconds of arc. The validation, discussed in the results section, consisted in comparing computed LOS deviations with those measured experimentally. The experimental measurement of LOS deviations was made at Ames for the Gemini window with the actual Gemini edge supports and with clamped and simply supported edges. In the experiment, an actual Gemini window in its frames was mounted in a pressure tank to simulate the actual in-flight pressure environment. The window was also mounted in the pressure tank in special frames that simulated the idealized clamped and simply supported edge conditions. The test equipment, an interferometer, consisted of a gas laser, mirrors, and other related instrumentation. The experimental measurement technique and the results of the experimental study are discussed in reference 7.

RESULTS

All results presented in this section were obtained for a window having three panes of glass, with the same size and shape and of the same material as the Gemini window.

The LOS deviations discussed in this section include the combined effects of pressure deformation, wedge angle, and the index of refraction difference. Both in-plane and out-of-plane deviations will be presented.

Total LOS Deviations for Clamped and Simply Supported Edges

The structural analysis program (SAMIS) was used to compute the window surface pressure deformations for these edge conditions.

In-plane deviations.- The total in-plane deviations, $\Delta\delta$, are presented in figures 3(a) and 3(b) as a function of y-axis position for several incidence angles with azimuth angle $\alpha = 270°$. The y-axis position is defined as that point on the y-axis where the incident ray intersects the xy-plane of the coordinate system. This term will be used extensively throughout the Results section. In general, the in-plane deviations increased in magnitude with increasing incidence angle and as the distance from the center of the optical area increased. Deviations for clamped edges are larger than for the simply supported edges. The deviations reached a maximum of about 18 arcsec.

In-plane deviations for various azimuth angles, at $\theta = 45°$, are presented in figures 3(c) and 3(d) for clamped and simply supported window edges. Deviations for clamped and simply supported edges exhibit similar trends with the deviations somewhat larger for the clamped edged case. For both edge conditions, the largest deviations were obtained for 0° and 180° azimuth angles and the smallest deviations were for 270° azimuth.

Out-of-plane deviations.- Out-of-plane deviations, $\Delta\alpha$, are shown in figures 4(a) and 4(b) for several incidence angles and for $\alpha = 270°$. Deviations for the clamped edges (fig. 4(a)) are less than 0.5 arcsec in magnitude for all cases ($\theta = 5°$ to 45°) and for the simply supported edges (fig. 4(b)) are less than 2 arcsec in magnitude in all cases.

Out-of-plane deviations for various azimuth angles and for $\theta = 45°$ are presented in figures 4(c) and 4(d). The clamped and simply supported edge deviations exhibit very similar characteristics with the simply supported edge deviations slightly larger, reaching a maximum of about 8 arcsec for $\alpha = 225°$ and $Y = 1.0$.

Comparison of computed (SAMIS) LOS deviations for clamped and simply supported edges with experimentally measured data.- In order to validate the accuracy of the computed LOS deviations for clamped and simply supported edge conditions, the computed data were compared with the experimental data of reference 7. It should be noted that the experimental data in reference 7 cannot be compared directly with the computed data presented here since they are in different coordinate systems. An appropriate coordinate transformation was performed to put the experimental data in the proper coordinate system. A comparison of typical computed and experimental in-plane LOS deviations is shown in figure 5. As indicated in reference 7, the experimental data are accurate to ±1 arcsec. LOS deviations are presented as a function of y-axis incidence position for two incidence angles and for $\alpha = 270°$. Clamped edge data are shown in figure 5(a) and simply supported edge data in figure 5(b). The maximum difference between computed and experimental LOS deviations for the data shown is about 3 arcsec, which is typical of all the data obtained. Out-of-plane deviations, which are not shown, exhibited similar differences. The computed and experimental data for these edge conditions were compared in detail by determining the difference, D, between the computed and experimental LOS deviations for all the x, y incidence positions tested and for all combinations of azimuth and elevation angles. That is, $D = \Delta_E - \Delta_C$, where Δ_E is the experimentally measured LOS deviation for a

particular combination of incidence position, azimuth angle, and elevation angle, and Δ_C is the computed LOS deviation for the same conditions. A detailed statistical analysis was performed by computing the mean and standard deviations of the differences between computed and measured LOS deviations. Differences were analyzed as functions of the incidence angle, θ, and the azimuth angle, α, for all x, y positions. All three edge conditions were analyzed for both in-plane and out-of-plane deviations. The mean difference, $\overline{D}$, is given by

$$\overline{D} = \frac{\sum_{i=1}^{n} D_i}{n}$$

and the standard deviation of the differences, S_D, is given by

$$S_D = \frac{\sum_{i=1}^{n} D_i^2 - n\overline{D}^2}{n - 1}$$

where i represents a particular combination of x, y position, azimuth angle, and elevation angle. It should be emphasized that the mean difference is the mean of the differences between computed and experimental LOS deviations, where the differences are obtained by subtracting the experimental LOS deviation from the computed LOS deviation for the same x, y, α, and θ. The quantity $(n - 1)$ is used in the determination of S_D rather than n because it provides an unbiased estimate of the true standard deviation, as indicated in references 11 and 12. The standard deviation in this form is used in navigation for trajectory and space position estimation. Since the results obtained by our method are intended for application to navigation systems, the $(n - 1)$ term was used in this report.

The mean difference, $\overline{D}$, and the standard deviation, S_D, of the in-plane LOS deviations are presented in figure 6 for the two edge conditions.

In figure 6(a), the mean difference is given as a function of incidence angle, θ, for $\alpha = 270°$ and 9 x, y positions. The mean difference varies from about 1 to 4 arcsec. In figure 6(b), the mean difference is given as a function of azimuth angle for $\theta = 45°$ for the same x, y positions. Here the mean difference data show considerable variation with change in azimuth angle for both the clamped and simply supported edges, ranging from -1 to -10 arcsec for clamped edges and from +3 to -10 arcsec for simply supported edges.

The standard deviation, S_D, of the differences is given as a function of incidence angle, θ, for $\alpha = 270°$ in figure 6(c). Generally, S_D increases as θ increases. The standard deviations are the smallest for the clamped edges (<2 arcsec). Standard deviations are given as a function of azimuth

angle in figure 6(d) for $\theta = 45°$. Generally, they are less than 2.5 arcsec and exhibit little variation with azimuth angle.

The mean differences and standard deviations of the out-of-plane LOS deviations for the two edge conditions are presented in figure 7. In figure 7(a), the mean difference is given as a function of incidence angle for $\alpha = 270°$. For this azimuth angle, the mean differences are generally larger than for the in-plane deviations, reaching a maximum of about 8 arcsec for clamped edge with $\theta = 15°$. The mean differences tend to decrease with increasing θ. Mean differences as a function of azimuth angle are presented in figure 7(b) for $\theta = 45°$. In this case, the mean differences vary considerably with azimuth angle for the clamped and simply supported edge conditions, ranging between -4 and +6 arcsec.

Standard deviations are presented in figure 7(c) as a function of θ for $\alpha = 270°$. They increase with increasing θ for the clamped edge and have little variation with θ for the simply supported edge. The standard deviations are given as a function of azimuth, α, for $\theta = 45°$ in figure 7(d). The standard deviations vary between 1 and 3 arcsec.

If all the experimental and computed LOS deviation data for clamped and simply supported edges for all combinations of incidence position, azimuth angle, and incidence angle are considered, the in-plane LOS deviations have a mean difference from -2 to -3 arcsec and a standard deviation of 3 to 4 arcsec. The out-of-plane deviations have a mean difference from 1 to 2 arcsec and a standard deviation of 4 to 5 arcsec.

These statistics are based on a total of 240 data points, each corresponding to a particular azimuth angle, elevation angle, and position on the y-axis.

These results indicate that most of the LOS deviations for these edge conditions agree with the experimentally measured data to within a few arcsec. The in-plane deviations varied from -1 to +20 arcsec and the out-of-plane deviations varied from -7 to +8 arcsec.

Comparison of Deviations for a Simply Supported Edge Based on Pressure Deformations Obtained From the Structural Analysis Program and From Interference Photos

As previously discussed, if the edge conditions are known, surface pressure deformations can be obtained from the structural analysis program. It has been shown that LOS deviations based on the pressure deformations obtained from the structural analysis program agree well with experimentally measured data. However, if the spacecraft window edge conditions are not known or not easily defined, which is true of the Gemini window, an alternative method must be used to determine the pressure deformations. One method is to measure the pressure deformations from interference photographs of the window surfaces. The pressure deformations for the Gemini window with simply supported edges were obtained from interference photographs. These pressure deformations were then used in the computation of LOS deviations. In

figure 8, the in-plane LOS deviations obtained by this method are compared with the line-of-sight deviations based on pressure deformations obtained with the structural analysis program. The interference photo data are represented by the dashed lines, and the data based on the structural analysis program are represented by the solid lines. The data from the structural analysis program are taken from figures 3(b) and 3(d). In figure 8(a), the deviations are given for various incidence angles with $\alpha = 270°$. In figure 8(b), the deviations are given for various azimuth angles with $\theta = 45°$. The two sets of data agree to within about an arcsec for values of Y between 1.25 and -1.25. The fringes near the edges of the interference photographs were extremely close together and thus very difficult to discern, even with good magnifying equipment. The out-of-plane deviations that are not shown exhibited similar agreement. It appears that the interference photograph method of determining pressure deformations can provide good results.

Total LOS Deviations for Actual Gemini Edges

Total LOS deviations computed for the Gemini window with actual Gemini edge conditions, on the basis of window surface pressure deformations measured from interference photographs, are presented in figures 9 and 10.

In-plane deviations.- The total in-plane LOS deviations are presented in figures 9(a) and (b) as a function of y-axis position. In figure 9(a), deviations are shown for several incidence angles with $\alpha = 270°$. As the distance from Y = 0 increases, the deviations tend to increase in magnitude, attaining a maximum of about 16 arcsec. In figure 9(b), deviations are shown for several azimuth angles and $\theta = 45°$. Deviations show considerable variation, ranging from -7 to +16 arcsec.

Out-of-plane deviations.- Total out-of-plane deviations are presented in figures 9(c) and 9(d) as a function of y-axis position. In figure 9(c), deviations are given for several incidence angles with $\alpha = 270°$ for nine x, y positions. Deviations vary between 0 and 6 arcsec but exhibit little variation with change in incidence angle. In figure 9(d), the deviations are given for several azimuth angles and $\theta = 45°$ for the same x, y positions. Again, the deviations exhibit considerable variation, ranging between -10 and +7 arcsec.

Comparison of computed LOS deviations for actual Gemini edges with experimentally measured data.- The LOS deviations computed for the actual Gemini edges on the basis of pressure deformations obtained from interference photos are compared with experimentally measured data in figure 10. In-plane deviations are compared in figure 10(a) for two incidence angles with $\alpha = 270°$. The deviations agree quite well to within 1 arcsec. Out-of-plane deviations are shown in figure 10(b) for the same incidence and azimuth angles. Out-of-plane deviations agree to within about 4 arcsec.

The computed and experimentally measured LOS deviations for the actual Gemini edges were compared in detail. A statistical analysis of the differences between the computed and experimentally obtained data, both in-plane and out-of-plane, is presented in figures 11 and 12, respectively. This

analysis is similar to that in figures 6 and 7 for clamped and simply supported edges. In figure 11(a), the mean difference between computed and experimental data is shown as it varies with incidence angle for $\alpha = 270°$. The mean difference increases as θ increases but is always less than 2 arcsec. In figure 11(b), the mean difference for $\theta = 45°$ is shown as it varies with change in azimuth angle. The mean difference varies between ±2 arcsec.

In figure 11(c), the standard deviation of the mean difference for $\alpha = 270°$ is given as a function of θ. The standard deviation increases with increasing θ and reaches a maximum of 2.7 arcsec. In figure 11(d), the standard deviation is shown for $\theta = 45°$ as a function of α and varies from 1.4 to 3.6 arcsec.

In figures 12(a) and 12(b), the mean difference between computed and experimental out-of-plane deviations is presented. In figure 12(a), the mean difference is given for $\alpha = 270°$ as a function of θ. The mean difference decreases with increasing θ and varies between 1.5 and 4.8 arcsec. In figure 12(b), the mean difference is given for $\theta = 45°$ as a function of α. The mean difference ranges from 0.8 to 4.8 arcsec.

In figures 12(c) and 12(d), the standard deviation of the mean differences is presented. In figure 12(c), the standard deviation is shown for $\alpha = 270°$ as a function of θ. The standard deviation also decreases with increasing θ and varies from 1.5 to 2.8 arcsec. In figure 12(d), the standard deviation for $\theta = 45°$ is shown as a function of α and varies between 0.8 and 3.3 arcsec.

If all the data for actual Gemini edges are considered, the mean difference for the in-plane deviations is 0.5 arcsec and the standard deviation is 2.0 arcsec. For out-of-plane deviations, the mean difference is 3 arcsec and the standard deviation about the mean is 3 arcsec. These statistics are based on 120 data points.

This statistical analysis indicates that the analysis method based on pressure deformations taken from interference photos and used to compute the LOS deviations for actual Gemini edges accurately determined the LOS deviations to within a few arcsec.

The Effect of Models on LOS Deviations

It has been demonstrated in the preceding sections that the computed LOS deviations compared quite well with experimental data. However, when these comparisons of data were made, it was noted that in a few cases relatively large differences existed between computed and experimental data. Mean differences up to -10 arcsec for in-plane deviations and up to 8 arcsec for out-of-plane deviations were obtained in some cases. These fairly sizable differences might be attributed to inaccuracies in the models of the window surfaces used in the analysis. These inaccuracies could result from incorrect information about the nonflatness, wedge angle, or pressure deformations.

To illustrate the effect of inaccuracies in the models, an additional 2-arcsec wedge angle was added to each windowpane of the model for simply supported edge conditions. The thick part of the wedge angle was toward the positive x-axis of the coordinate system. LOS deviations were then recomputed with this new model and the new results were compared with the experimental data. The comparison showed that the modification changed the in-plane deviations as much as 5 arcsec.

The net effect of adding the additional wedge angle was to move the analytically determined data closer to the experimentally measured data. It appears then that the relatively large differences between analytically determined and experimentally measured data that occur in a few cases might be attributed in part to inaccuracies in the window surface model used in the analysis. It is emphasized that extreme care must therefore be exercised in the determination of the window surface models.

Individual Parameter Effects and Sextant Errors

Individual LOS deviations.- As part of this study, LOS deviations that would result from variations of each individual parameter, such as window nonflatness, wedge angle, and pressure loading, were also computed. The deviations computed for the individual parameters are of interest because they give insight into the relative importance of each parameter from the standpoint of spacecraft window design.

Convex and concave window surfaces resulted in small deviations, but biconvex and biconcave surfaces exhibited large deviations - up to 90 arcsec. LOS deviations due to wedge angle reached a maximum of about 10 arcsec, while pressure loading led to deviations up to 13 arcsec. Individual LOS deviations are considered in detail in appendix A.

Linear superposition.- After the LOS deviations caused by the individual parameters had been computed, it was of interest to combine the individual deviations for a particular combination of nonflatness, wedge angle, and pressure bowing by linear superposition. These LOS deviations were then compared with the deviations computed with a math model that included the combined effects of nonflatness, wedge angle, and pressure loading. From this comparison, linear superposition was not considered valid in this application.

CONCLUDING REMARKS

Methods have been formulated for predicting LOS deviations induced by spacecraft windows. The methods were used to compute the LOS deviations associated with a three-pane Gemini spacecraft window with three edge conditions: the actual Gemini edges and idealized clamped and simply supported edges. Single LOS deviations, in-plane and out-of-plane, were presented for the three edge conditions. These deviations included the combined effects of window surface nonflatness, wedge angle, and pressure deformation, as well as index-of-refraction difference of the light transmission media inside and

outside the spacecraft. The deviations presented are functions of both LOS orientation and incidence position on the window. In-plane deviations up to 20 arcsec and out-of-plane deviations up to 17 arcsec were encountered. The largest in-plane deviations were obtained for clamped edges.

The computed LOS deviations were compared with experimentally measured LOS deviations in order to assess the validity of the methods developed. A detailed statistical analysis of the differences between computed and experimentally measured data indicated that the results agreed to within -1.5 arcsec mean difference and 3.4 arcsec standard deviation for in-plane deviations. Out-of-plane deviations agreed within 2 arcsec mean difference with a standard deviation of 4 arcsec. Some relatively large differences between computed and experimentally measured data exist. These differences could be attributed, at least in part, to inaccuracies in the models of the window surfaces used in the study. It is felt that the methods developed would accurately predict spacecraft window-induced LOS deviations if the window surface shapes can be accurately determined.

The LOS deviations associated with the individual parameters, such as window surface nonflatness, wedge angle, and pressure loading, were also investigated. Convex and concave window surfaces results in small deviations, but biconvex and biconcave surfaces exhibited large deviations - up to 90 arcsec. LOS deviations due to wedge angle reached a maximum of about 10 arcsec, while pressure loading led to deviations up to 13 arcsec.

Ames Research Center
National Aeronautics and Space Administration
Moffett Field, Calif., 94035, April 10, 1969
125-17-02-13-00-21

APPENDIX A

INDIVIDUAL PARAMETER LOS DEVIATIONS

LOS deviations that result from variations of individual parameters, such as window surface nonflatness, wedge angle, and pressure loading, are of interest because they may give insight into the problems of spacecraft window design. Thus, LOS deviations for the following individual math models were obtained for the 6-inch optical area of the three pane Gemini window: (1) pressure deformation only; (2) nonflatness only; and (3) wedge angle only. The math model for pressure deformations was obtained with the structural analysis program. A pressure environment that corresponded to the orbiting Gemini spacecraft was assumed. Math models were obtained for clamped and simply supported edge conditions.

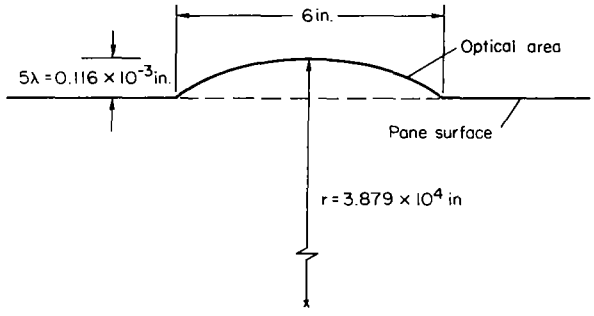

Sketch (h)

The math models for nonflatness and wedge angle were based on the assumption that the window just met the Gemini specifications, that is, both surfaces of each pane having five wavelengths nonflatness and with a 4-arcsec wedge angle. It was further assumed that the nonflatness was spherical in nature (sketch (h)). LOS deviations were obtained for windows having all three panes convex toward the inside of the spacecraft, all three panes concave, all three panes biconvex, and all three panes biconcave.

The math models for wedge angle assumed that the thick part of the wedge was either at the top or the bottom of the window. Sketch (i) defines the two angles, i and r, required to describe the wedge angle in the math model, where i is the angle that the surface of the windowpane makes with the xy-plane and r is the angle that the intersection of the window surface and the xy-plane makes with the x-axis. For this discussion, i = 4 arcsec and r = 0. Figures 13 through 16 present computed LOS deviations caused by the individual parameters. In all cases, the in-plane deviations are shown.

Flatness

LOS deviations for windows having nonflatness only and wedge angle only are presented in figure 13.

In figures 13(a), (b), and (c), the window surfaces were assumed to be spherical with a 5λ maximum surface deviation from the flat reference plane. In figure 13(a), deviations are presented as a function of y-axis position for several azimuth angles (incidence angle $\theta = 45°$) for a window

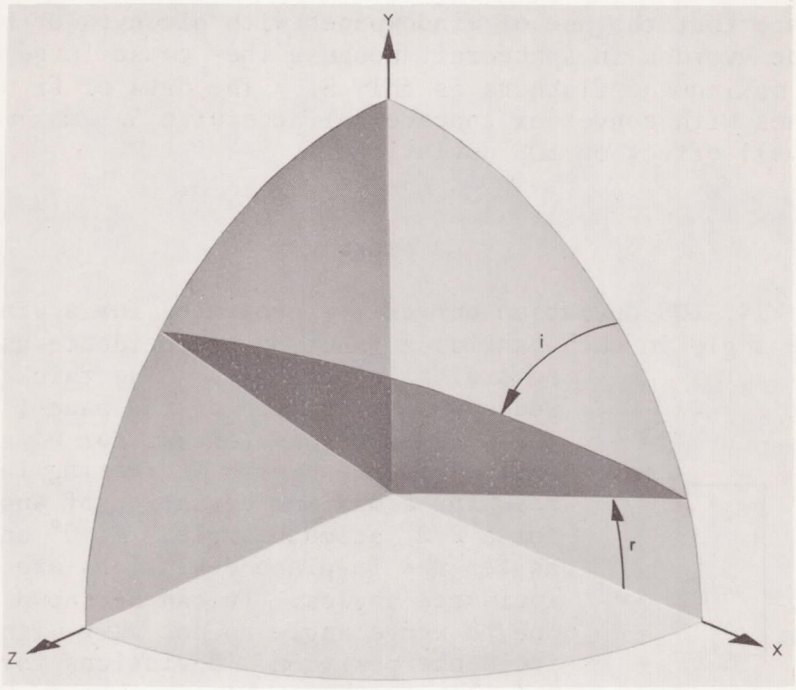

Sketch (i)

having all three panes with biconvex surface shapes (sketch (j)). The deviations vary linearly with change in position and reach a maximum of 85 arcsec at 270° azimuth and $y = -2.5$. In figure 13(b), the LOS deviations are presented as a function of y position for several angles of incidence and for $\alpha = 270°$. Again, the deviations vary linearly with change in position and generally increase in magnitude with increasing incidence angle. The LOS deviation of windows with biconcave surfaces (sketch (j)) would equal that computed for the biconvex surfaces, but would be opposite in sign.

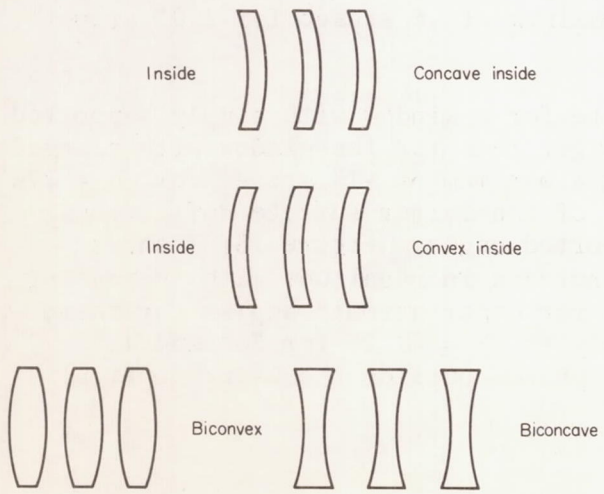

Sketch (j)

In figure 13(c), deviations are presented as a function of incidence angle for a window with all three panes convex toward the inside of the spacecraft and for a window with all three panes concave toward the inside of the spacecraft (sketch (j)). The LOS deviations are less than 3 arcsec and increase in magnitude with increasing incidence angle. Since the surface nonflatness is spherical, it can be shown that the LOS deviations vary as a function of incidence angle only.

At this point, the data of figures 13(a), (b), and (c) can be summarized. Results of figures 13(a)

and (b) indicate that the use of windowpanes with biconvex or biconcave surfaces should be avoided in spacecraft because they cause large LOS deviations even when the maximum nonflatness is only 5λ. The data of figure 13(c) show that windowpanes with convex or concave surfaces with 5λ maximum nonflatness have only a small effect on LOS deviations.

Wedge

In figure 14, LOS deviation curves are presented for a window with a 4-arcsec wedge angle in each pane as a function of incidence angle and for several azimuth angles. The thick part of the wedge was at the top of the pane (sketch (k)). The LOS deviations (except for 0° and 180° azimuth angles) increase with increasing incidence angle, reaching a maximum deviation of about 10 arcsec for a 270° azimuth angle. At 0° and 180° azimuth angles the in-plane deviations are zero for all incidence angles. It can be shown that deviations due to wedge angle do not vary with change in incidence position. Deviations for a window with a 4-arcsec wedge angle, with the thick part of the wedge at the bottom of the windowpane, would be the same as those in figure 14, but with opposite sign.

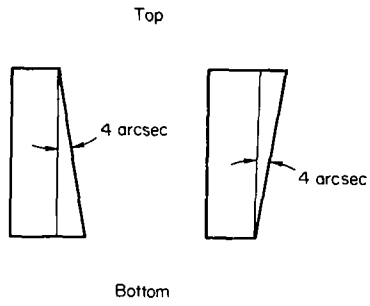

Sketch (k)

Pressure Loading

LOS deviations caused by pressure loads on the window similar to loads imposed on an orbiting Gemini vehicle (sketch (g)) are presented as a function of y-axis position in figure 15. The deflection of the window due to the pressure load was computed by means of the structural analysis program previously discussed. The data in figures 15(a) and (b) are for a window with clamped edges. The deviations reach a maximum of -6 arcsec for 270° azimuth angle and 45° incidence angle.

The data in figures 15(c) and (d) are for a window with simply supported edges. Generally, the deviations are larger than for the window with clamped edges under similar conditions, reaching a maximum of -13 arcsec for $\alpha = 270°$ and $\theta = 45°$. This is probably a result of the larger surface deflections that occur for a window with simply supported edges. Figure 15(d) shows that for $\alpha = 270°$, the LOS deviations increase in magnitude with increasing incidence angle. This trend also exists for other azimuth angles for these incidence positions. The data extend only to $Y = -1.25$ for 30° and 45° incidence angles, since the deviated ray passes outside the 6-inch optical area where the model is valid.

Index of Refraction

Deviations caused by the index of refraction difference between the air inside and the space vacuum outside the Gemini spacecraft are shown as a function of incidence angle in figure 16. The LOS deviation increases with increasing incidence angle and reaches 21 arcsec for $\theta = 45°$.

REFERENCES

1. Smith, Donald W.: The Hand-Held Sextant - Results From Gemini XII and Flight Simulator Experiments. AIAA Paper 67-775.

2. Murtagh, T. B.; Price, C. R.; and Smith, H. E.: Analysis of Gemini 7 - Star Sightings Utilizing a Space Sextant in Gemini 6. J. Spacecraft Rockets, vol. 4, no. 5, May 1967, pp. 567-572.

3. Silva, R. M.; Jorris, T. R.; and Vallerie, E. M., III: The Air Force Space Navigation Experiment on Gemini (DOD/NASA Gemini Experiment D-9, Gemini IV and VII Flights). AFAL-TR-66-289, Sept. 1966, U. S. Air Force Systems Command, Air Force Avionics Lab.

4. Schneider, Alan M.; Prussing, John E.; and Timin, Mitchell E.: A Manual Method for Space Rendezvous Navigation and Guidance. AIAA Paper no. 68-859

5. White, Kenneth C.; and Gadeberg, Burnett L.: Description of an Analytic Method for the Determination of Spacecraft Window-Induced Navigation Sighting Errors. Proceedings of the ION National Space Meeting on Simplified Manned Guidance, Navigation and Control, February 19-21, 1968, Cocoa Beach, Florida, pp. 180-195.

6. Walsh, Thomas M.; Warner, David N., Jr.; and Davis, Michael B.: The Effects of a Gemini Left-Hand Window on Experiments Requiring Accuracy in Sighting or Resolution. NASA TN D-3669, 1966.

7. Warner, David N., Jr.; and Walsh, Thomas M.: Effects of Edge Constraints on Optical Qualities of a Spacecraft Window. NASA TN D-4845, 1968.

8. Koch, Donald G.; Johnson, Patricia L.; and Hegemeier, G. A.: Gemini Window Optical Analysis. EOS Report 6141-Final, Electro Optical Systems, Contract NAS2-2495, November 1964.

9. Gadeberg, Burnett L.; and White, Kenneth C.: The Theory of the Correction of Celestial Observations Made for Space Navigation or Testing. NASA TN D-5239, 1969.

10. Melosh, R. J.; Diether, P. A.; and Brennan, M.: Structural Analysis Systems Usage Report. WDL-EM 73. Philco Corp., Palo Alto, Calif., NAS7-100, JPL Contract No. 950321. NASA CR-60975, July 1963.

11. Eshbach, O. W.: Handbook of Engineering Fundamentals. John Wiley and Sons, Inc., 1936, p. 2-123.

12. Mood, A. M.: Introduction to the Theory of Statistics. McGraw-Hill Book Co., Inc., 1950, p. 156.

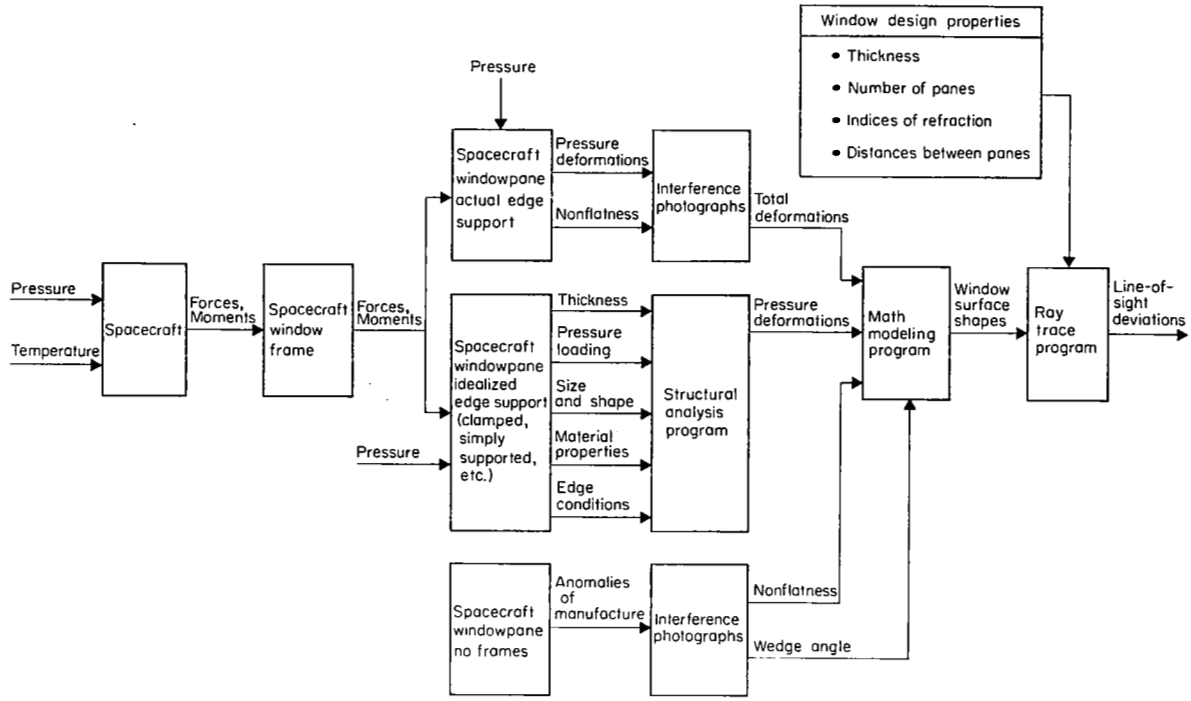

Figure 1.- Window analysis method.

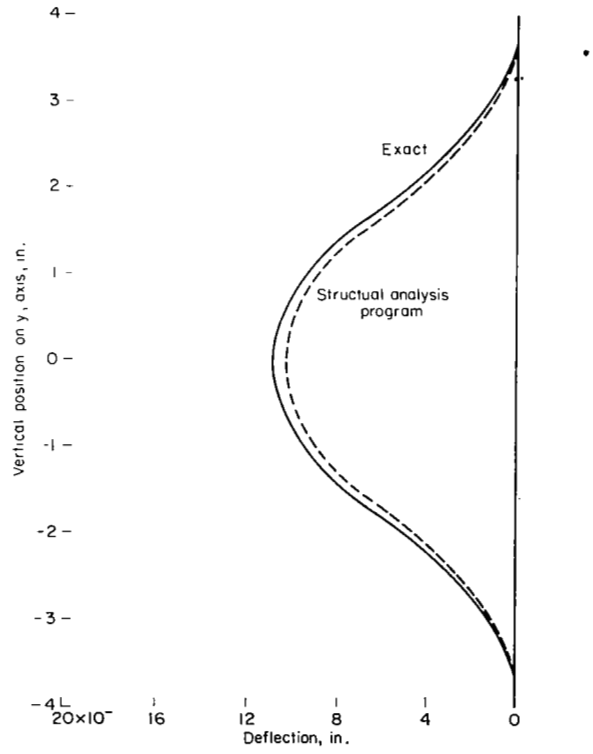

Figure 2.- Comparison of exact solution and structural analysis program deformations for an ellipse with clamped edges.

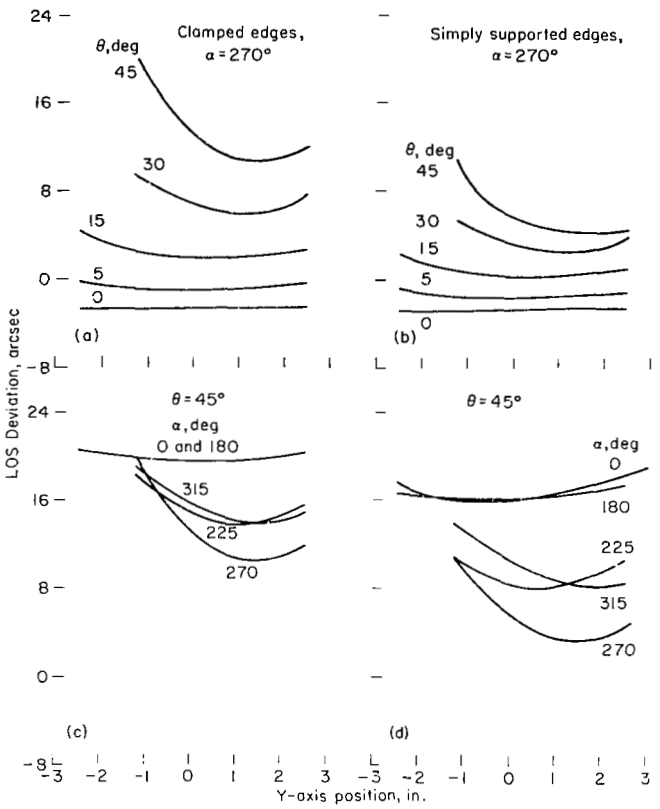

Figure 3.- Total computed (SAMIS) in-plane LOS deviations for clamped and simply supported edge conditions.

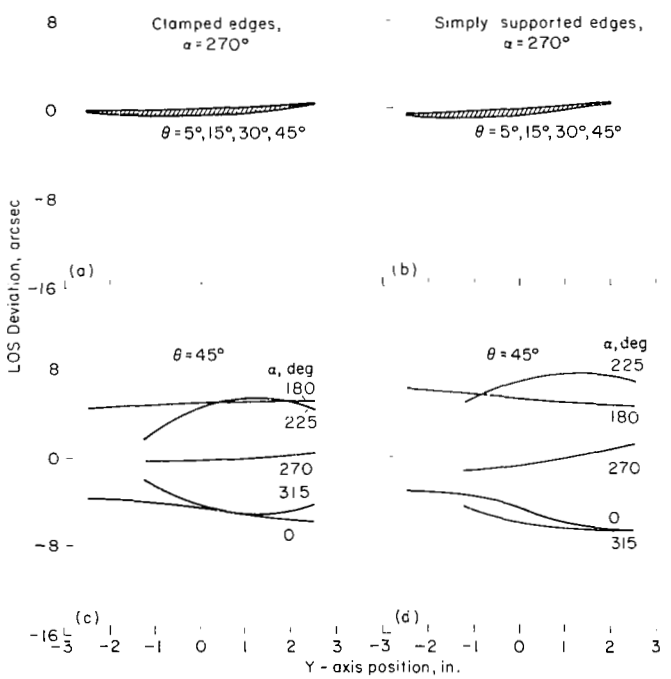

Figure 4.- Total computed (SAMIS) out-of-plane LOS deviations for clamped and simply supported edge conditions.

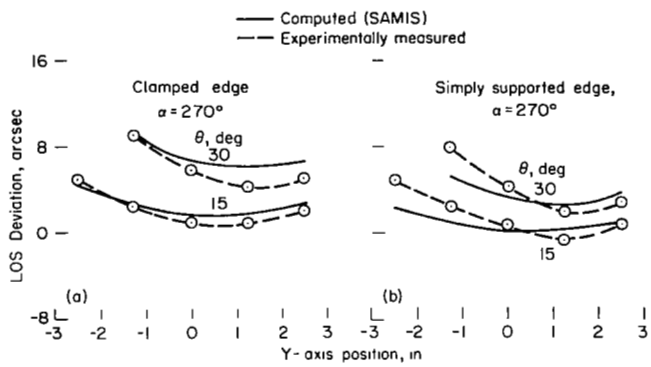

Figure 5.- Comparison of computed (SAMIS) and experimentally measured in-plane LOS deviations for clamped and simply supported edges.

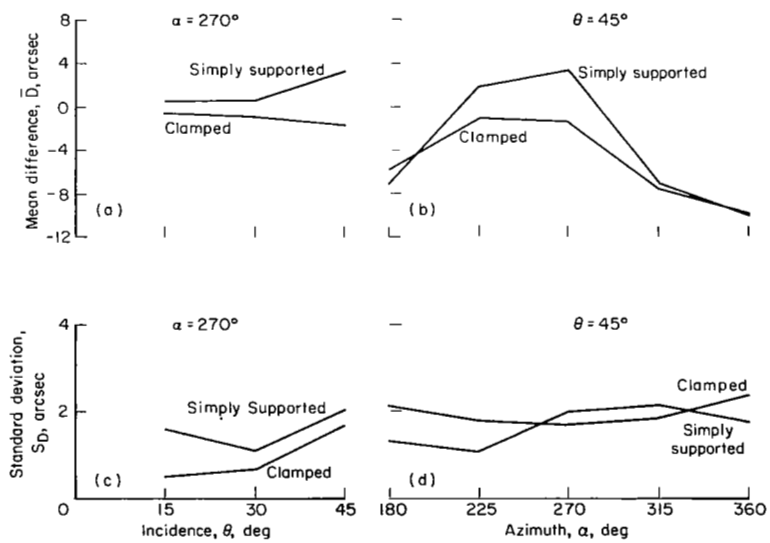

Figure 6.- Mean differences and standard deviations of the mean differences between computed (SAMIS) and experimentally measured total in-plane LOS deviations.

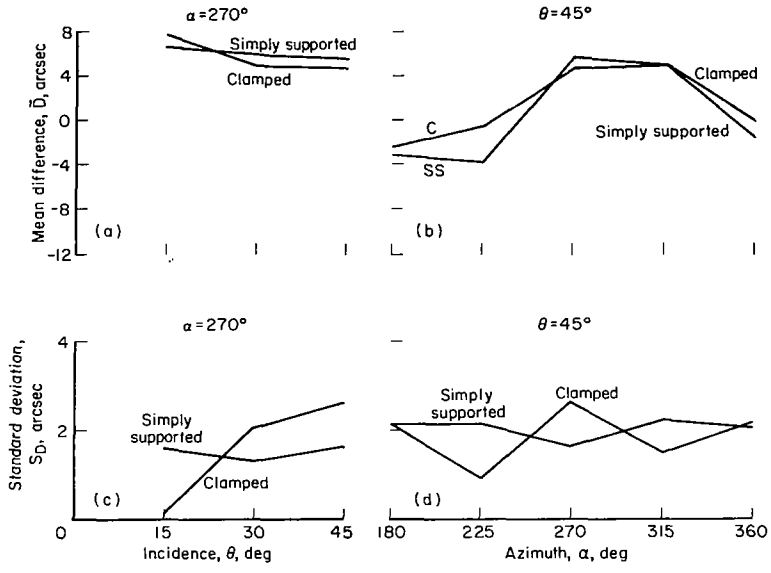

Figure 7.- Mean differences and standard deviations of the mean differences between computed (SAMIS) and experimentally measured total out-of-plane LOS deviations.

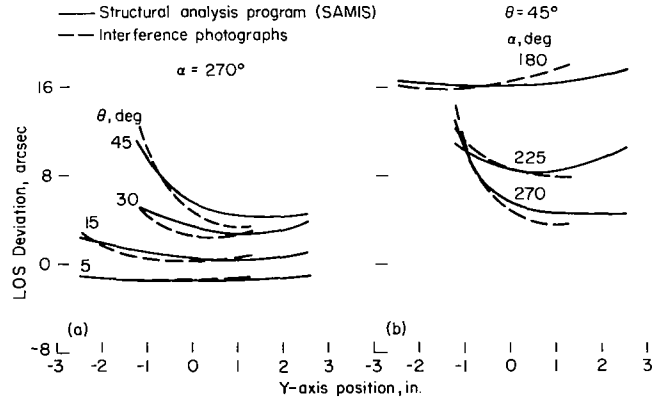

Figure 8.- Comparison of in-plane LOS deviations for free edge.

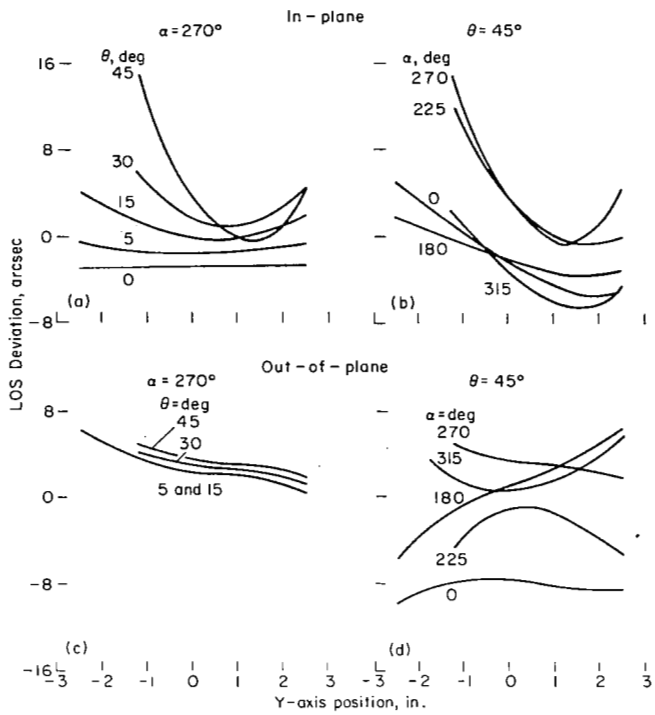

Figure 9.- Total computed (int. photos) LOS deviations for actual Gemini edges.

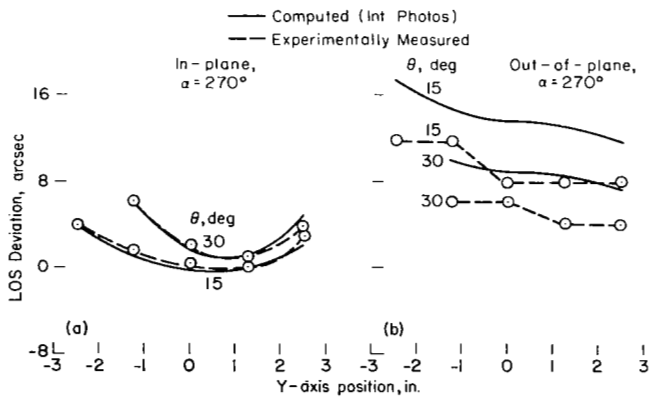

Figure 10.- Comparison of computed (int. photos) and experimentally measured LOS deviations for actual Gemini edges.

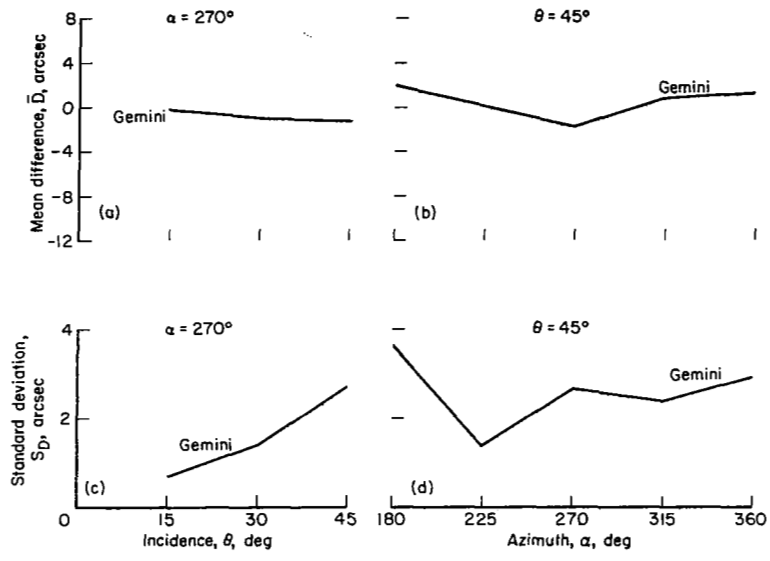

Figure 11. Mean differences and standard deviations of the mean differences between computed (int. photos) and experimentally measured total in-plane LOS deviations for actual Gemini edges.

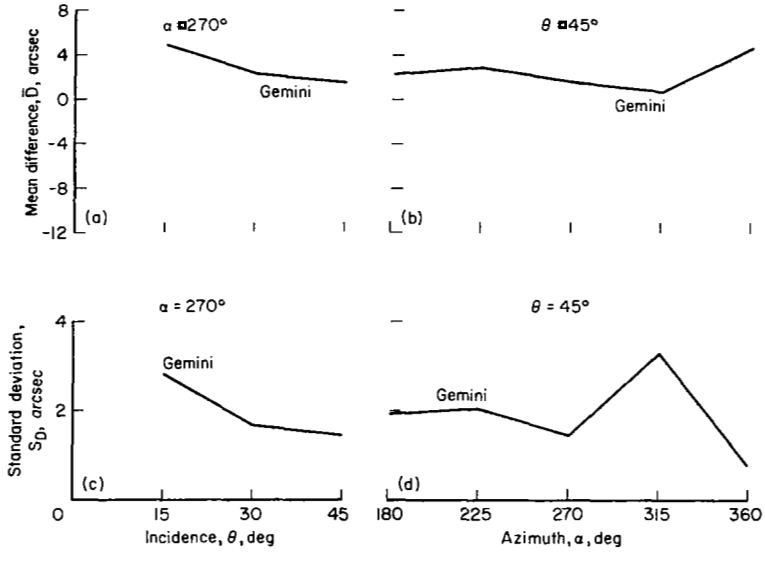

Figure 12.- Mean differences and standard deviations of the mean differences between computed (int. photos) and experimentally measured total out-of-plane LOS deviations for actual Gemini edges.

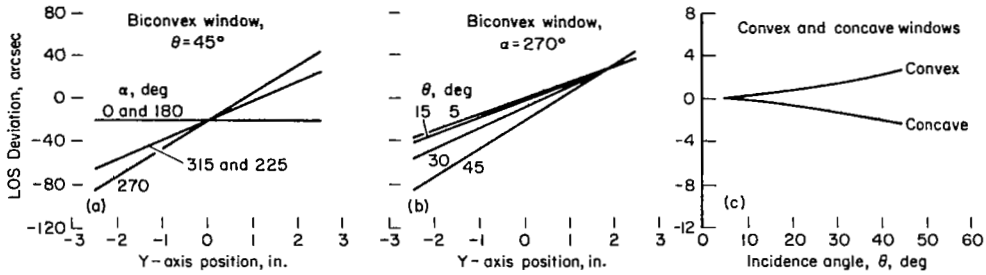

Figure 13.- Nonflatness and wedge angle line-of-sight deviations.

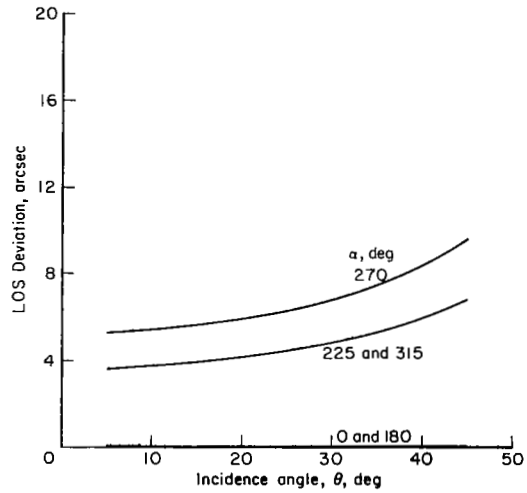

Figure 14.- LOS deviations, wedge angle.

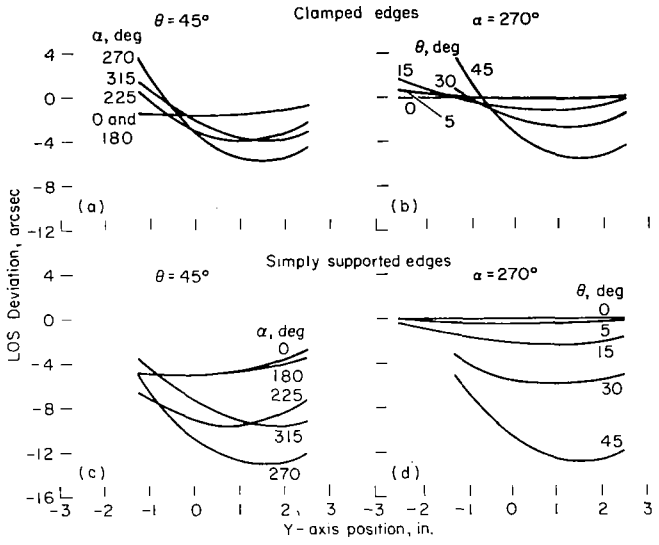

Figure 15.- Pressure loading line-of-sight deviations.

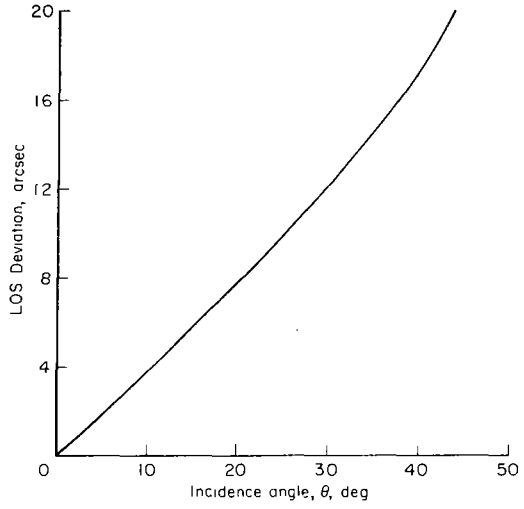

Figure 16.- Index of refraction difference line-of-sight deviations.

"The aeronautical and space activities of the United States shall be conducted so as to contribute . . . to the expansion of human knowledge of phenomena in the atmosphere and space. The Administration shall provide for the widest practicable and appropriate dissemination of information concerning its activities and the results thereof."

—NATIONAL AERONAUTICS AND SPACE ACT OF 1958

NASA SCIENTIFIC AND TECHNICAL PUBLICATIONS

TECHNICAL REPORTS: Scientific and technical information considered important, complete, and a lasting contribution to existing knowledge.

TECHNICAL NOTES: Information less broad in scope but nevertheless of importance as a contribution to existing knowledge.

TECHNICAL MEMORANDUMS: Information receiving limited distribution because of preliminary data, security classification, or other reasons.

CONTRACTOR REPORTS: Scientific and technical information generated under a NASA contract or grant and considered an important contribution to existing knowledge.

TECHNICAL TRANSLATIONS: Information published in a foreign language considered to merit NASA distribution in English.

SPECIAL PUBLICATIONS: Information derived from or of value to NASA activities. Publications include conference proceedings, monographs, data compilations, handbooks, sourcebooks, and special bibliographies.

TECHNOLOGY UTILIZATION PUBLICATIONS: Information on technology used by NASA that may be of particular interest in commercial and other non-aerospace applications. Publications include Tech Briefs, Technology Utilization Reports and Notes, and Technology Surveys.

Details on the availability of these publications may be obtained from:

SCIENTIFIC AND TECHNICAL INFORMATION DIVISION

NATIONAL AERONAUTICS AND SPACE ADMINISTRATION

Washington, D.C. 20546